Simulation Study of the Correlation between Structure and Conductivity in Stretched Nafion

Elshad Allahyarov*

Department of Physics, Case Western Reserve University, Cleveland, Ohio 44106, and Joint Institute of High Temperatures, Russian Academy of Sciences (IVTAN), Moscow 125412, Russia

Philip L. Taylor

Department of Physics, Case Western Reserve University, Cleveland, Ohio 44106

Received: May 30, 2008; Revised Manuscript Received: October 14, 2008

We have used coarse-grained simulation methods to investigate the effect of stretching-induced structure orientation on the proton conductivity of Nafion-like polymer electrolyte membranes. Our simulations show that uniaxial stretching causes the hydrophilic regions to become elongated in the stretching direction. This change has a strong effect on the proton conductivity, which is enhanced along the stretching direction, while the conductivity perpendicular to the stretched polymer backbone is reduced. In a humidified membrane, stretching also causes the perfluorinated side chains to tend to orient perpendicular to the stretching axis. This in turn affects the distribution of water at low water contents. The water forms a continuous network with narrow bridges between small water clusters absorbed in head group multiplets. In a dry membrane the side chains orient along the stretching direction.

I. Introduction

In their role as proton-conducting membranes, ionomers are an important component of many hydrogen fuel cells. In these materials, the interplay among the short-range interactions between the hydrophobic backbone polymer and the hydrophilic terminal groups and the long-range Coulomb interactions between the electrostatic charges on the terminal groups and the protons induces a nanophase separation into proton-rich and proton-poor domains. A general model for the phase morphology of ionomers has been proposed by Eisenberg et al.,[1] according to which a few head groups combine to form multiplets that restrict the mobility of the backbone chain segments directly attached to them. A spherical geometry is often assumed for these multiplets, whose sizes are typically less than a nanometer.[2] The average distance between these multiplets is mostly dictated by the concentration of head groups relative to that of backbone monomers. These multiplets then form microdomains, and one observes a microphase separation that can serve to facilitate proton diffusion. Recent experimental data on the morphology of ionomers describe the aggregations as elongated objects embedded in a continuous ionic medium.[3] A goal of much ionomer research is to increase the proton conductivity, and hence to make membranes that can operate under very low humidity conditions, as a higher conductivity results in a higher output power density in fuel cells containing these membranes.

Proton conduction itself is a complex process, which strongly depends on the thermal and mechanical history of the membrane.[4−6] The mechanical history involves the manufacture of the membrane, which is usually achieved by one of two common procedures: solution casting[7,8] or extrusion.[9] The former method is used to make membranes from a solution of dissolved ionomer by allowing the solvent to evaporate from the solution. While this technique is suitable only for small-scale laboratory production, it has the advantage producing isotropic membranes with no residual preferential orientation of their backbone within the plane of the membrane.

Most commercially available ionomeric membranes are fabricated by extrusion of a molded sample. This leads to a preferred orientation of the ionomer backbone,[10] the extent of which depends on the draw speed of the extrusion. This inherent structural anisotropy of the backbone matrix is believed to be a reason for the susceptibility to tearing or cracking of the membrane in any swelling or drying processes. This creates technical problems in keeping the membrane taut in the changing temperature−humidity conditions encountered in fuel cells. An equally important issue concerns the effect of this anisotropy on proton conductivity. While it has generally been assumed that such effects are significant, the problem of predicting the consequences of mechanical strain remains largely unsolved.

There have been several experimental studies in which membranes were uniaxially stretched in order to probe the effects of strain on internal morphology. Gebel et al.[11] analyzed the form of ionic domains in unstretched and stretched membranes and showed that mechanical stretching induces ordering in the ionomer backbones. Elliot et al.[12,13] detected the anisotropy in stretched membranes by performing scattering experiments. Barbi et al.[10] used membrane elongation measurements to confirm the classical ionomer domain model, in which inverted micelles are interconnected by channels. As expected, uniaxial stretching of recast Nafion causes a preferential orientation of the Nafion backbone in the direction of stretching, and this is morphologically similar to the anisotropy in extruded membranes. Cable et al.,[14] for example, stretched Nafion and found the proton conductivity to be higher in the plane of the membrane than normal to it. A slightly different result was found by Lin et al.,[15] who noted little change in transverse conductivity on stretching but found an improved fuel cell performance, as compared to Nafion 117 and unstretched recast Nafion, as a

* To whom correspondence should be addressed.

10.1021/jp8047746 CCC: $40.75
Published on Web 12/30/2008

consequence of a lowered methanol permeation rate. In a related experiment, Elabd et al.[16] measured the conductivities of an ionic block copolymer and observed appreciable anosotropy. Oren et al.[17] found that the conductivities of membranes could be rendered anisotropic through the alignment of suspended particles, with higher conductivity in the alignment direction. These studies reveal the significant impact that organized and oriented structures can have in increasing proton conductivity. While there have been several intensive simulation studies of the hydrated morphology on transport properties of Nafion or Nafion-like membranes,[18−25] there are no studies of which we are aware of the effects of mechanical stretching on an equilibrated sample.

In this paper we investigate numerically to what extent induced orientation in the backbone polymer affects proton diffusion and conductivity in Nafion-like ionomers. The nature of our united-atom model for the ionomer is described in section II, and the details of our simulation procedure are given in section III. Section IV reports our results for stretch-induced morphological changes in the ionomer, while results for the proton conductivity are given in section V. In section VI we discuss our conclusion that stretching of solvated membranes leads to anisotropy of the conductivity, with the stretch-induced ordering of the backbone increasing the longitudinal protonic conductivity while decreasing the transverse conductivity.

II. Model

Because it is necessary to model quite large volumes of material in order to see the types of morphological changes in which we are interested, it is unfortunately not feasible to perform fully atomistic simulations. We thus employ the same united-atom model for Nafion[21,22,26] as was used in our previous work.[27] Within this approach the CF_2 and CF_3 groups of the backbone and side chains, the ether oxygens of the side chain, the sulfur atom, and the O_3 oxygen group of the sulfonates are modeled as Lennard-Jones (LJ) monomers of diameter $\sigma = 3.5$ Å. All the ether oxygens and fluorocarbon groups are assigned zero partial charges. The electrostatic charges are located entirely on the SO_3^- sulfonate head groups and on the H^+ protons.

The total potential energy of the system is then given as

$$U_{\text{total}} = U_{\text{LJ}} + U_q + U_{\text{bond}} + U_{\text{angle}} + U_{\text{dihedral}} \quad (1)$$

Here the first two terms on the right-hand side are pair interactions between nonbonded monomers. The first term is the Lennard-Jones interaction

$$U_{\text{LJ}}(r) = 4\varepsilon_{\text{LJ}} \sum_{i>j} ((\sigma/r_{ij})^{12} - a(\sigma/r_{ij})^{6}) \quad (2)$$

where $\varepsilon_{\text{LJ}} = 0.2$ kcal/mol and $r_{ij} = |\vec{r}_i - \vec{r}_j|$ is the separation distance between monomers i and j. At a temperature of 300 K, this value of ε_{LJ} would correspond to an energy of about $k_BT/3$. The parameter a is 1 for hydrophobic−hydrophobic (HH) interactions and 0.5 for both hydrophobic−hydrophilic (HP) and hydrophilic−hydrophilic (PP) interactions between monomers. In the PP case, the LJ potential was modified to be purely repulsive by truncating it at its minimum, where $r = 1.122\sigma$, and raising it by the addition of an amount ε_{LJ}.

These interaction parameters were chosen to agree in most instances with the Nafion model of Paddison et al.[28] and Spohr et al.[29] We note that the adoption of a single diameter σ for all monomers and a single LJ interaction parameter ε_{LJ} for Nafion makes the simulation of our model more tractable. The different values of a in eq 2, discussed above, discriminate between the attractive HH, slightly attractive HP, and completely repulsive PP interactions between Nafion monomers. Our united atom model can be easily expanded to fully hydrophobic or fully hydrophilic membranes by choosing only one value for the parameter a in eq 2.

The electrostatic interaction between charged sulfonate groups and protons is

$$U_q = \sum_{i>j} \frac{q_i q_j e^2}{\varepsilon(r_{ij}) r_{ij}} \quad (3)$$

Here q_l ($l = i, j$) is +1 for protons, +1.1 for sulfur atoms, and −2.1 for the combined oxygens of the sulfonate groups, thus ensuring that the total charge of a sulfonate head group SO_3^- is $-e$. The distance-dependent dielectric permittivity $\varepsilon(r)$ in eq 3 reflects the fact that, at small separations, there is no intervening material between any two charges. There is then no screening of the Coulomb interaction, and the effective permittivity is close to unity. At modest distances the charges will be separated by matter that may be water, ionic groups, or backbone polymer, and the energy of interaction will be reduced by the shielding effect of this material. The interaction between sulfonates, both inside the sulfonate head group clusters surrounded by polymeric matrix, and between two different sulfonate clusters separated by polymeric matrix is thus a complicated function that includes the effects of image charge distributions at the boundaries.[30] When water is present, dielectric saturation and water immobilization effects in the hydrophilic phases of the ionomeric membrane[31,32] add complications. While the best approximation for $\varepsilon(r)$ is still a matter for debate,[33] it is clear that the permittivity must increase with distance. We choose the form $\varepsilon(r) = 1 + \varepsilon_B((r/\sigma - 1)/(r/\sigma + 1))$[10], which smoothly increases from $\varepsilon = 1$ near a chosen charge to being the dielectric permittivity ε_B of the bulk at large distances. Dielectric measurements based on a bulk response of the membrane to an electric field in the microwave region[34,35] show an increase of bulk ε from 4 to 20 as λ changes between 1 and 16. For higher hydration levels[36] the average dielectric permittivity of the membrane approaches the value 30. These changes in permittivity are related to the contribution of different water states in the membrane: bound, free, and intermediate.[35] Since the maximal hydration level considered in this work is $\lambda = 5$, we use $\varepsilon_B = 8$ in our simulations, in accordance with the experimental results of ref 35. For simplicity, we consider the same value of ε_B for all the membrane states simulated in the current work. The dielectric saturation effects can be evaluated directly in simulations via calculation of water polarization inside small systems. There are available data on the dielectric saturation of water versus the distance from the pore center in the membrane.[37,38] These calculations show the existence of bulklike water in the center of the pore and a strong dependence of the overall distance-dependent permittivity on the intrusion of the sulfonates and on the distribution of the sulfonates on the pore walls.[39] Because of the fact that there is no explicit pore structure in our model Nafion membrane, our choice of a distance-dependent permittivity qualitatively follows the trend of dielectric saturation effects: it smoothly increases from 1 toward ε_B over a nanometer distance.

The effective dielectric permittivity ε_{eff}, calculated as a volume average of $\varepsilon(r)$ over a typical multiplet domain, appears to be in good agreement with reported dielectric constants for ionomers in ref 7.

The last three terms on the right side of eq 1 represent the potential energy of the bonded segments of the molecules. The two-body bond-stretching potential

$$U_{\text{bond}}(R) = \frac{1}{2} \sum_{\text{all bonds}} k_b(R - R_0)^2 \quad (4)$$

has a simple Hookean form with stretching constant $k_b = 700$ kcal/(mol Å^2) (roughly 1200 k_BT/Å^2 at room temperature) and unstretched bond length $R_0 = 1.54$ Å (0.44σ). For the three-body angle-bending potential

$$U_{\text{angle}}(\theta) = \frac{1}{2} \sum_{\text{all bond pairs}} k_\theta(\theta - \theta_0)^2 \quad (5)$$

we use an equilibrium bending angle $\theta_0 = 110°$ and a bending force constant $k_\theta = 120$ kcal/(mol deg^2) (or about 200 k_BT/deg^2). Finally, the dihedral (four-body) component of the total energy is written as

$$U_{\text{dihedral}}(\phi) = \frac{1}{2} \sum_{\text{all bond triplets}} k_\phi(1 - d\cos(3\phi)) \quad (6)$$

with the parameters having values $d = -1$ (+1) and $k_\phi = 18.1$ kcal/mol $\sim$ 10.8 k_BT (6.2 kcal/mol $\sim$ 3.7 k_BT) for backbone (side chain) segments, respectively.

We consider two models for the ionomer. In the first model, which is a highly simplified representation of a completely dry membrane, each proton is permanently attached to a sulfonate group. Each side-chain head group is thus electrostatically neutral and consists of two dipoles, connected head to tail. We refer to this as the bound-proton model.

In the second, and more realistic, model, the proton is more loosely bound to its sulfonate counterion by a Coulomb attraction. We refer to this as the solvated model. The activation energy needed to overcome the electrostatic attraction between the oppositely charged H^+ and SO_3^- ions, and thus detach the proton, depends on the average distance between sulfonates and on the water content λ in the membrane. This parameter λ is defined as the number of water molecules per sulfonate head group and varies between 0 and 25 for solvated membranes.

It is known that $\lambda \geq 5$ is sufficient to loosen the bonds tying the protons to the head groups and to achieve full dissociation. These free protons contribute to the conductivity principally through vehicular (sometimes called en-masse) diffusion and through the Grotthuss mechanism. There is still ongoing debate which of these mechanisms is the dominant contributor to the conductivity. Classical molecular dynamics simulations are capable of evaluating only the vehicular component of proton (hydronium) diffusion. A special treatment of hydrogen bonds has to be used for modeling the Grotthuss-type shuttling of protons. Simulations of a planar pore in Nafion with a simplified empirical valence-bond method for the hydrogen-bond network, implemented by Seeliger et al.,[40] show the prevailing role of Grotthuss diffusion when λ is in the range between 5 and 10. An improved multiscale empirical valence-bond method, applied by Blake et al.,[19] reveals an anticorrelation between vehicular and Grotthuss mechanisms. An ab initio approach for the hydrogen network, described by Devanathan et al.,[24] shows a strong binding of hydronium to sulfonates at low hydration, which, as a consequence, prevents vehicular transport. A prevalence of Grotthuss diffusion over vehicular transport is also reported by Thompson et al.[41] Choi et al.,[42] and Hristov et al.[25] for a wide range of hydration parameters λ. At low λ, the chain flexibility contributes to the surface hopping mechanism of protons with or without the involvement of water molecules.[41] There is also evidence that even one water molecule per sulfonate ($\lambda = 1$) is enough to dissociate the sulfonic groups.[43]

We use a simple point charge (SPC) fluid[20,44] to model the water molecules in our simulations. These move in a medium having a distance-dependent dielectric permittivity $\varepsilon(r)$ that we assume to be independent of λ. This includes the case of $\lambda = 0$, where in the absence of SPC water molecules the proton conductivity occurs only through the hopping mechanism. We notice that in this case the proton can be assumed to be a hydronium ion according to results of ref 43.

III. Simulation Details

The simulations were performed in stages. The first step was to grow a continuous backbone with attached pendant side chains by using Monte Carlo techniques. The bond length and the bending and dihedral angles for this initial polymer were fixed to be R_0, θ_0, and ϕ_0, respectively. After molecular dynamics (MD) runs of a few picoseconds, which were used to equilibrate the system, as this usually needed to respond to the strong steric repulsion of overlapping monomers, the constraints on angles and bonds were removed. Following this, the side chains were detached from the backbone skeleton in an approach previously adopted by Vishnyakov,[45] and the backbone skeleton was cut into segments.[46] This greatly increases the relaxation rate of the ionomer and allows a rapid equilibration of the system. The system then consists of $N_s = 1000$ side chain segments and $N_b = 1400$ backbone segments. Taking into account that the sulfonic acid groups are hydrophilic while the ethers and fluorocarbon groups are hydrophobic,[28] we adopted the following coarse-grained representation. The side-chain architecture is written as $7H + 3P$ for a dry membrane and $7H + 2P$ for a humidified membrane. In the latter case the hydrogen atom is detached from the side chain and thus considered a free hydrophobic charge. Here the letters H and P stand for hydrophobic and hydrophilic monomers, respectively. The backbone segments are fully hydrophobic with a $14H$ architecture.

Molecular dynamics runs with a Langevin thermostat were performed for the segmented polymer for time periods up to 50 ps in a constant-NVT ensemble. We imposed periodic boundary conditions for a cube of side $L = 30\sigma$ and used the Lekner summation method[47] to handle the long-range electrostatic interactions between charged particles. In order to verify that the system had not become trapped into a metastable glassy state, we repeated each run with several different initial configurations.

In the next stage of the simulations, the segments were reassembled back into the branched chain characterizing the original Nafion. This was achieved by the simultaneous introduction of the bonds and angular constraints described by eqs 4−6 between the ends of each backbone segment, which united them into a single chain. Similar bond and angular constraints between the tail monomer of each detached side chain and the median monomer of every backbone segment connected the side chains to the backbone polymer. To avoid the formation of starlike branched polymers, only a single occupancy of the backbone attachment sites was permitted. The unequal numbers of backbone segments and side-chain segments resulted in the formation of a polymer in which there were varying numbers of backbone monomers between the points of attachment of the side chains. The simulation was then resumed

and run until a new equilibrium was achieved. Once the system was fully equilibrated, the statistically averaged quantities of interest were gathered during the next 2−3 ns of run time for the initial case of unstretched membranes.

As a test of this procedure, we ran simulations for solvated membranes in which we did not adopt the procedure of detaching the side chains and then reattaching them, but instead left them intact. After a very long time the system did reach a point where the results were equivalent to those achieved much more rapidly in the earlier procedure. However, for a completely dry system, for which the membrane is best approximated by an attached-proton model for the side chains, even long simulations of several nanoseconds duration were not enough to achieve a completely equilibrated system. It is similarly difficult to mimic existing experimental procedures for membrane equilibration, such as casting the membrane from dilute solution, or gradual quenching of high-temperature ionomers down to room temperature. Hence, we acknowledge that the procedures implemented in this work for quick equilibration of a randomly generated ionomer might bias the head group cluster formation, in both unstretched and stretched states. Proton diffusion and dissociation from the head groups might also possibly be affected, as considered by Paul[48] and by Padison.[49]

The stretched samples were constructed by the application of a set of forces designed to emulate the effects of a longitudinal stress. The continuous backbone polymer was considered as a set of N_b connected segments, and a weak force $\mathbf{f}_\pm$ was applied to the end monomer of each segment. The direction of this force was in the positive z direction for the end with the greater value of its z coordinate and in the negative z direction for the end with the lesser value of its z coordinate in an extended-zone scheme where the periodic boundary conditions were not applied. This force tends to align the backbone segments in the z direction without having significant influence on the side-chain dynamics. The strength of $\mathbf{f}_\pm$ was restricted to values much smaller than the forces arising from the bond, angle, and dihedral potentials.

It usually took 50 ps to equilibrate the stretched membrane under constant stress. Following this, runs of 2−3 ns were performed to gather statistically significant results for the morphology of the stretched material. For studies of proton conductivity, an external electric field of 10^8 V/m was applied to thermally equilibrated and mechanically stretched membrane. Then additional 50 ps runs were performed to reach steady-state conditions before nonequilibrium MD (NEMD) simulation runs of 2−3 ns were undertaken. In this way the effects of both mechanical stretching and applied fields could be determined. The simulation results presented below correspond to stationary states. No morphological changes were detected during the production runs or during additional runs with start-up configurations taken from the final structures of previous 2−3 ns runs. We note that one must be alert to the possibility of field-induced structural changes in the ionomer when transport characteristics are evaluated. This concern was very recently addressed by Yan et al.,[50] who investigated a small all-atomistic Nafion system and found non-Maxwellian velocity distributions at strong applied fileds, indicating large drift velocities of the ions. In contrast, our ion drift velocities never exceeded 20 m/s, which is a small fraction of the kinetic velocity, and our speed distributions were Maxwellian. This discrepancy most likely arises from our use of a Langevin thermostat but may also reflect our use of coarse graining, a large system size, and a large number of protons. Our pair correlation analysis of the ionomer density shows no field-induced changes in the structure of head groups, in line with results of Chen.[51] Such changes only arise in our simulations at fields above 10^9 V/m. In order to suppress field-induced macroscopic membrane movement, a constraint was applied to suppress the total momentum of all components other than the free charge carriers.

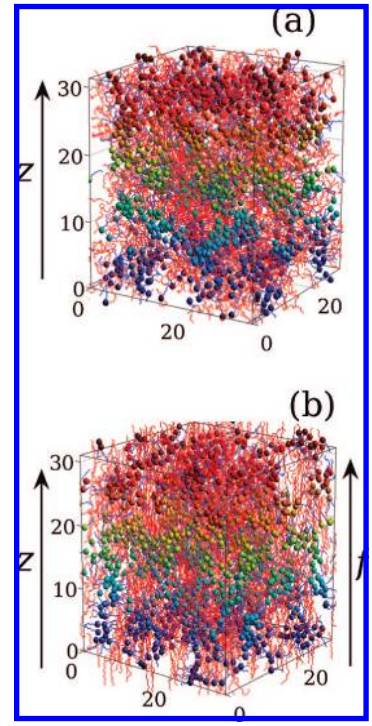

Figure 1. Typical snapshot of the simulation box for (a) unstretched ($f = 0$) and (b) stretched ($f = 1$) Nafion membrane with water content $\lambda = 3$. The stretching force f in (b) is directed along the z axis. Colored beads represent the end-group oxygens of side chains. Pendant side chains and neutral backbone polymer are drawn by lines (blue and red, respectively). Different bead colors correspond to different bead altitudes, with blue for beads at the bottom of the simulation box and red for beads at the top of the box. The size of all structural elements is schematic rather than space-filling.

IV. Results for Stretched-Membrane Morphology

A snapshot of an equilibrated membrane with a water content of $\lambda = 3$ molecules per head group and in the absence of an applied stretching force is given in Figure 1a. The hydrophobic backbone and the side chains are shown as lines (red and blue, respectively). The spheres indicate the sulfonate head groups of the side chains and show clusterlike aggregations of different sizes and shapes, in agreement with experimental observations.[52] A moderately stretched membrane with dimensionless stretching force $f = 1$ is shown in Figure 1b. This corresponds to an actual force on each chain segment of 190 pN, which is in the range capable of unfolding polymers[53] or unzipping DNA.[54] The polymer backbone shows ordering in the direction of the applied force, which is parallel to the z axis. We determine the induced backbone ordering S_b and side-chain ordering S_s by calculating the order parameter

$$S_j = \frac{1}{2}\left(3\left\langle \frac{1}{N_b}\sum_{i=1}^{N_b}\cos^2\theta_i \right\rangle - 1\right) \qquad (7)$$

an approach commonly used in liquid crystal systems. Here j = b, s for the backbone polymer and side chains, respectively, the angular brackets $\langle ... \rangle$ denoting statistical averaging over the

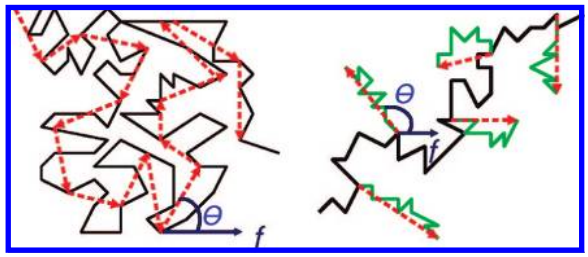

Figure 2. This schematic illustration explains the calculation of order parameters S_b for backbones (left picture) and S_s for side chains (right picture). The continuous black line represents the backbone polymer of the ionomer. Shorter green lines represent the side chains. The dashed lines are vectors constructed to show the orientation of backbone segments and side chains, with θ being the angle between the orientation vector and stretching direction.

NVT ensemble. The orientational angle θ for each segment is defined as the angle between the vector connecting the first and last monomers of the segment and the applied force **f**, as illustrated in Figure 2. The backbone matrix is considered as a set of N_b segments of 14 monomers each. In a similar manner we define the orientational angle θ for side chains as also shown in Figure 2. Here θ is the angle between the stretching force **f** and the vector pointing from the first monomer of the side chain toward its terminal group.

The order parameters S_b and S_s, calculated from eq 7, are shown in Figure 3. As expected,[10−13] membrane stretching leads to ordering in the ionomer conformation. The backbone ordering, shown in Figure 3a, is greatest in the bound-proton model and decreases in the solvated case as the water content λ increases for a fixed force **f**. Figure 3b reveals the completely different response of the side chains to the stretching force. When the bound-proton membrane is stretched, the side chains tend to orient themselves parallel to the stretching force. However, when a solvated membrane is stretched, the side chains are more likely to be perpendicular to the stretching force, in accord with previous experimental results.[55] A possible explanation for these different responses to stress lies in the effect of the humidity on multiplet formation. In the absence of water, the dipolar interactions between sulfonates leads to the formation of dense multiplets containing 10−20 terminal groups, as seen in Figure 4a. The Coulomb forces of attraction between these dipoles limit the amount of molecular relaxation of the side chains in response to stretching. The backbone deformation is thus followed by the rearrangement of multiplets via elongation in one direction and shrinking in the other direction. This is evident from a comparison of the curves for stretched and unstretched membranes in Figure 4a. The sulfur−sulfur pair distribution function decreases when the membrane is in a stretched state. The vertical lines in Figure 4 are drawn to show the multiplet diameter, the distance at which the $g_{SS}(r)$ descends to unity. It is clear that, when stretched, the diameter of these disk-shaped terminal clusters shrinks as a consequence of their elongation along the stretch direction. In contrast, when the membrane is solvated, the water content lowers the densities of the multiplets. These then coalesce to form larger clusters in which a mixture of solvent molecules and conducting protons gives the head groups more dynamic flexibility. As a result, the side chains can achieve a gain in entropy by rearranging themselves perpendicular to the direction of the applied stress. This is the reason why only a slight deformation of the multiplet geometry for the solvated membrane is seen in Figure 4b. In summary, the order parameter of the membrane depends on its hydration level, the absorbed solvent being an obstacle for the backbone ordering S_b but facilitating the side-chain ordering S_s.

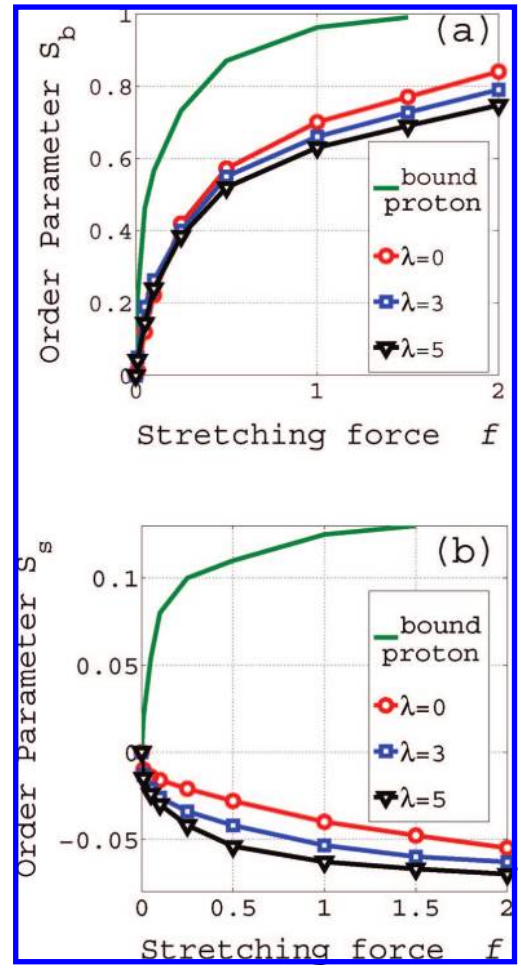

Figure 3. Backbone order parameter S_b (a) and side-chain order parameter S_s (b) as functions of applied stretching force f for the bound-proton model and for different water contents λ. $f = 1$ corresponds to stretching force 190 pN.

The most important aspect of the effect of stress on morphology concerns the formation of channels through which proton transport might occur. An indication of this is shown in Figure 5, in which the water distribution in a stretched ionomer is displayed. The water molecules congregate in elongated clusters in association with the distribution of side-chain head groups and are oriented in the direction of the applied stress. During the course of the simulation, the clusters create temporary bridging connections allowing the water to diffuse easily back and forth along the stretching direction. This morphology and dynamics of the water undoubtedly facilitate proton diffusion parallel to the stretching direction.

In order for proton conduction to occur, it is necessary for there to be a continuous network of pathways through the hydrophilic material in a membrane. This makes it useful to have a quantitative measure of the connectivity of the hydrophilic channels. To this end we have developed a method[56] aimed at detecting hydrophilic pathways in a network of hydrophilic clusters. The only input parameter for this method is the maximum separation distance parameter r_m between neighboring particles in the pathway. Our method calculates the distribution function $P(L_S)$ of the hydrophilic channel length L_S, which is defined as the distance between the initial and end points of the pathway. We applied this method to determine how the stretched-membrane morphology alters the channeling in the hydrophilic network of clusters. The distribution function $P(L_S)$ when r_m is chosen to be 2σ (which is 7 Å, the average

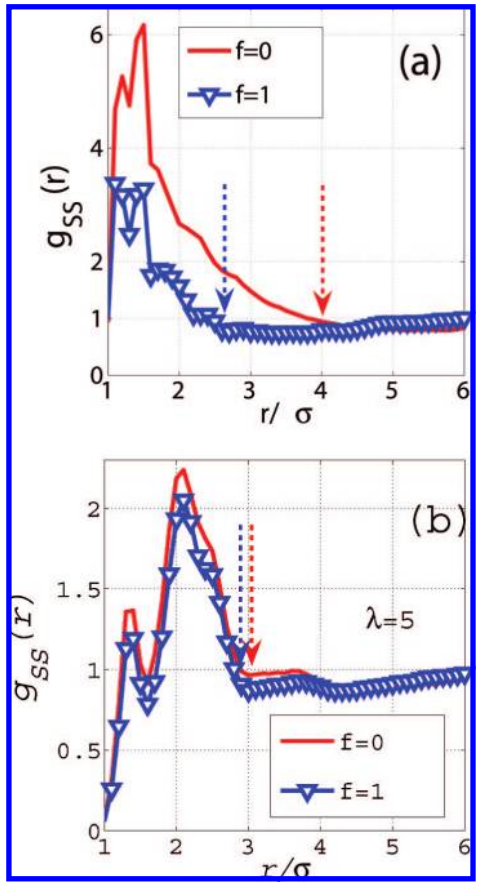

Figure 4. Effect of strain on the sulfur−sulfur pair distribution function $g_{SS}(r)$ for (a) the bound-proton model and (b) the solvated ionomer with $\lambda = 5$. Dashed arrows show the average size of multiplets.

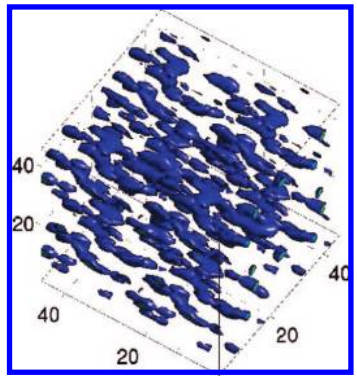

Figure 5. Instantaneous distribution of water clusters in a stretched, solvated membrane for stretching force $f = 1$ and water content $\lambda = 5$ water molecules per sulfonate.

separation between sulfonates in Nafion) is shown in Figure 6, for both stretched and unstretched membranes. Both curves have a similar short-range behavior and show a maximum at a most probable channel length equal to about 3σ. This is roughly the average size of the sulfonate multiplets in solvated membranes, as is seen in Figure 4b. The long-range behavior of $P(L_S)$, however, shows a dependence on the mechanical treatment of the membrane. In a stretched membrane the hydrophilic−sulfonic channels in the membrane are 50% longer than in an unstretched membrane. We note that the calculated $P(L_S)$ is an instantaneous measure of the pathways in a network of clusters. Because of the constantly changing patterns in the distribution, which are caused by the diffusion of ions and water and the motion of head groups, the real pathways are effectively longer and can

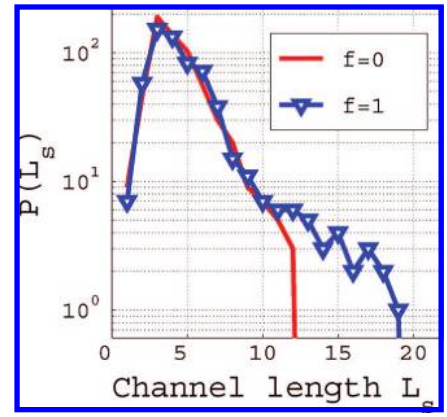

Figure 6. Distribution function $P(L_S)$ of sulfonate channel lengths L_S for unstretched ($f = 0$) and stretched ($f = 1$) solvated membranes having a water content $\lambda = 5$.

even traverse the whole system. Consequently, one expects that the protons in a stretched membrane can continuously travel along the stretching axis z. We explore the resulting protonic conductivities in the next section.

V. Results for the Conductivity of a Stretched Membrane

In this section we analyze the effect of membrane stretching on the protonic current. The electrical conductivity χ due to proton current in a solvated membrane can be obtained by performing NEMD simulations to find the current j in the presence of an external electrostatic field E through the relation

$$\mathbf{j} = \chi(\mathbf{E})\mathbf{E} \tag{8}$$

Here the induced current density $\mathbf{j}$ is given by

$$j = (1/V)\sum_{i=1}^{N_S} q_i v_{i,\mathbf{E}} \tag{9}$$

where $v_{i,\mathbf{E}}$ is the $\mathbf{E}$-field component of the velocity of the ith proton and N_S is the total number of protons in the system.

Because a strong applied electric field may itself have an effect on the morphology, we isolate the effects of stretching by examining only fields $\mathbf{E}$ at which the ionomer shows no structural changes. The longitudinal and transverse conductivities were evaluated by applying fields parallel and perpendicular to the stretching direction and extrapolating the resultant conductivities to find their values at zero applied field. The calculated values of χ_0 for the case where $\mathbf{E}$ is along the membrane stretching axis are shown in Figure 7 as a function of the membrane order parameter S_b for different solvation parameters λ. It is seen that ordering in the membrane backbone increases the conductivity, with a dependence of $\chi_0(S_b)$ on S_b that is close to being linear for all water contents λ. This finding is in accordance with experimental results of Cable et al.[14] Conversely, when we examine the transverse protonic conductivity χ_0 across the stretched membrane, which is shown in Figure 8, we find that the conductivity decreases with increasing backbone ordering. These two trends can be understood as a direct consequence of the channel-like nanophase separation along the stretching direction. While the protons can freely travel along these channels as a consequence of the water cluster bridging, there are no continuous pathways for them to travel across the

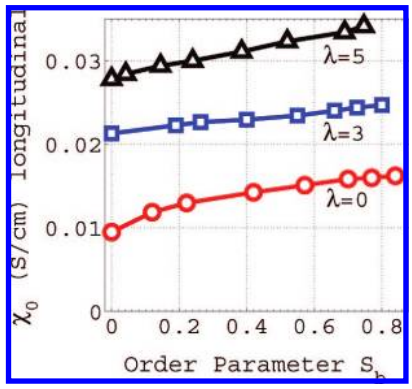

Figure 7. Protonic conductivity χ_0 of a stretched membrane along the stretching direction as a function of the backbone order parameter S_b for different membrane solvations. The water content parameters λ are indicated below the corresponding lines.

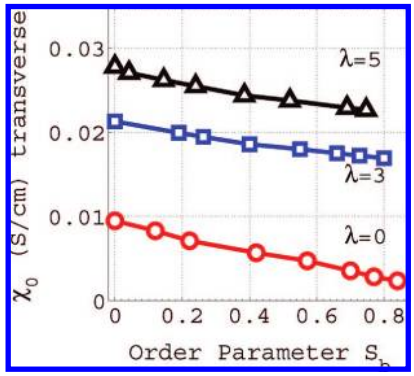

Figure 8. Protonic conductivity χ_0 of a stretched membrane perpendicular to the stretching direction as a function of the backbone order parameter S_b for different membrane solvations. The water content parameters λ are indicated below the corresponding lines.

stretching direction. This anisotropy in the conductivity is most pronounced in the drier samples.

VI. Discussion and Conclusion

The simulation results presented in the previous sections show that the uniaxial stretching of a Nafion-like ionomer should be expected to have a significant effect on its proton conductivity. The conductivity along the stretching direction is considerably higher than its value in an unstretched membrane, while the proton diffusion perpendicular to the stretching axis is strongly reduced. The anisotropy of conductivity of a stretched ionomer that we observe in our simulations is in accord with the measurements of Elabd et al.,[16] where a similar anisotropy of conductivity of an ionic block copolymer was reported.

When a water-containing sample is stretched, the perfluorinated side chains exhibit a tendency to be oriented perpendicular to the stretching force direction. The sulfonate clusters deform as the stretching is increased and show a long-range ordering in their distribution across the membrane. This affects the distribution of absorbed water, which forms a continuous network with narrow bridges.

The effect of the water is different for the backbone and side-chain ordering parameters. As seen from Figure 3, water is an obstacle to backbone ordering S_b parallel to the direction of elongation. However, water enhances the side-chain ordering S_s perpendicular to the stretching direction. For a given stretching force **f**, the order parameter S_b of the membrane backbone depends on the solvation parameter λ.

The simulations reported here were carried out at room temperature and under conditions of constant stress. We made no attempt to investigate how the anisotropy in the protonic conductivity depends on the temperature at which the membrane was stretched. Experimental measurements of crystallinity, however, indicate that membrane stretching at elevated temperatures can lead to different results from ambient-temperature stretching.[14,57] It appears that uniaxial extension of membranes at temperatures above the boiling temperature of water results in a material with an oriented morphology that persists after the samples are removed from the extensional stress. Also, higher temperature compression-molded ionomers exhibit a backbone crystallization when stretched.[58] It would thus be of interest to pursue further studies to enlarge on those presented here.

Finally, we note that with regard to the issue of improving fuel-cell performance by using stretched membranes our results indicate that the observed increased proton conductivity occurs only in the direction of stretching. As a practical matter, the desired direction of proton transport is across the membrane, and so the production of a membrane with enhanced conductivity due to stress may be difficult to arrange.

Acknowledgment. We acknowledge stimulating discussions with P. Pintauro and R. Wycisk, who introduced us to their membrane stretching experiments. E.A. thanks M. Litt for valuable comments on equilibrium ionomer morphologies. This work was supported by the US Department of Energy under Grant DE-FG02-05ER46244 and was made possible by use of facilities at the Case ITS High Performance Computing Cluster and the Ohio Supercomputing Center.

References and Notes

(1) Eisenberg, A.; Hird, B.; Moore, R. B. *Macromolecules* **1990**, *23*, 4098.
(2) Gohy, J. F.; Jerome, R.; van den Bossche, G.; Sobry, R. *Macromol. Chem. Phys.* **1998**, *199*, 2205.
(3) Rubatat, L.; Rollet, A.; Gebel, G.; Diat, O. *Macromolecules* **2002**, *35*, 4050.
(4) Yamamoto, Y.; Ferrari, M. C.; Baschetti, M. G.; De Angelis, M. G.; Sarti, G. C. *Desalination* **2006**, *200*, 636.
(5) Banerjee, S.; Curtin, D. E. *J. Fluorine Chem.* **2004**, *125*, 1211.
(6) Kim, M. H.; Glinka, C. J.; Grot, S. A. *Macromolecules* **2006**, *39*, 4775.
(7) Lin, H.-L.; Yu, T. L.; Huang, C.-H.; Lin, T.-L. *J. Polym. Sci., Part B: Polym. Phys.* **2005**, *43*, 3044.
(8) Moore, R. B.; Martin, C. R. *Macromolecules* **1988**, *21*, 1334.
(9) Slade, S.; Campbell, S. A.; Ralph, T. R.; Walsh, F. C. *J. Electrochem. Soc.* **2002**, *149*, A1556.
(10) Barbi, V.; Funari, S. S.; Gehrke, R.; Scharnagl, N.; Stribeck, N. *Polymer* **2003**, *44*, 4853.
(11) Gebel, G.; Diat, O. *Fuel Cells* **2005**, *5*, 261.
(12) Elliott, J. A.; Hanna, S.; Elliott, A. M. S.; Cooley, G. E. *Macromolecules* **2000**, *33*, 4161.
(13) Elliott, J. A.; Hanna, S.; Elliott, A. M. S.; Cooley, G. E. *Polym. Eng. Sci.* **2006**, *46*, 228.
(14) Cable, K. M.; Mauritz, K. A.; Moore, R. B. *Chem. Mater.* **1995**, *7*, 1601.
(15) Lin, J.; Wycisk, R.; Pintauro, P. N.; Kellner, M. *Electrochem. Solid-State Lett.* **2007**, *10*, B19.
(16) Elabd, Y. A.; Walker, C. W.; Beyer, F. L. *J. Membr. Sci.* **2004**, *231*, 181.
(17) Oren, Y.; Freger, V.; Linder, C. *J. Membr. Sci.* **2004**, *239*, 17.
(18) Cui, S.; Liu, J.; Selvan, M. E.; Keffer, D. J.; Edwards, B. J.; Steele, W. V. *J. Phys. Chem. B* **2007**, *111*, 2208.
(19) Blake, N. P.; Petersen, M. K.; Voth, G. A.; Metiu, H. *J. Phys. Chem. B* **2005**, *109*, 24244.
(20) Jang, S. S.; Molinero, V.; Cagin, T.; Goddard III, W. A. *J. Phys. Chem. B* **2004**, *108*, 3149.
(21) Wescott, J. T.; Qi, Y.; Subramanian, L.; Capehart, T. W. *J. Chem. Phys.* **2006**, *124*, 134702.
(22) Vishnyakov, A.; Neimark, A. V. *J. Phys. Chem. B* **2001**, *105*, 7830; **2001**, *105*, 9586.

(23) Venkatnathan, A.; Devanathan, R.; Dupuis, M. *J. Phys. Chem. B* **2007**, *111*, 7234.
(24) Devanathan, R.; Venkatnathan, A.; Dupuis, M. *J. Phys. Chem. B* **2007**, *111*, 8096.
(25) Hristov, I. H.; Paddison, S. J.; Paul, R. *J. Phys. Chem. B* **2008**, *112*, 2937.
(26) Yamamoto, S.; Jinnouchi, R.; Yamakawa, Sh.; Hyodo, Sh. *14th Int. Conf. Prop. Water Steam, Kyoto, Japan* 2004, 411.
(27) Allahyarov, E.; Taylor, P. L. *J. Chem. Phys.* **2007**, *127*, 154901.
(28) Paddison, S. J.; Zawodzinski, T. A. *Solid State Ionics* **1998**, *113*, 333.
(29) Spohr, E.; Kornyshev, A. A.; Commer, P. *J. Phys. Chem. B* **2002**, *106*, 10560.
(30) Iversen, G.; Kharkats, Yu. I.; Ulstrup, J. *Mol. Phys.* **1998**, *94*, 297.
(31) Kreuer, K. D.; Paddison, S. J.; Spohr, E.; Sschuster, M. *Chem. Rev.* **2004**, *104*, 4637.
(32) Paul, R.; Paddison, S. *Mater. Res. Soc. Symp. Proc.* **2001**, *677*, AA7.16.1.
(33) Taylor, P. L.; Xu, B. C.; Oliveira, F. A.; Doerr, T. P. *Macromolecules* **1992**, *25*, 1694.
(34) Paddison, S. J.; Reagor, D. W.; Zawodzinski, T. A. *J. Electroanal. Chem.* **1998**, *459*, 91.
(35) Lu, Z.; Polizos, G.; Macdonald, D. D.; Manias, E. *J. Electrochem. Soc.* **2008**, *155*, B163.
(36) Paddison, S. J.; Bender, G.; Kreuer, K. D.; Nicoloso, N.; Zawodzinski, Th. *J. New Mater. Electrochem. Syst.* **2000**, *3*, 293.
(37) Paul, R.; Paddison, S. J. *Solid State Ionics* **2004**, *168*, 245.
(38) Paul, R.; Paddison, S. J. *J. Chem. Phys.* **2001**, *115*, 7762.
(39) Paul, R.; Paddison, S. J. *J. Phys. Chem. B* **2004**, *108*, 13231.
(40) Seeliger, D.; Hartnig, C.; Spohr, E. *Electrochim. Acta* **2005**, *50*, 4234.
(41) Thompson, E. L.; Capehart, T. W.; Fuller, T. J.; Jorne, J. *J. Electrochem. Soc.* **2006**, *153*, A2351.
(42) Choi, P.; Jalani, N. H.; Datta, R. *J. Electrochem. Soc.* **2005**, *152*, E123.
(43) Laporta, M.; Pegoraro, M.; Zanderighi, L. *Phys. Chem. Chem. Phys.* **1999**, *1*, 4619.
(44) Chan, K.; Tang, Y. W.; Szalai, I. *Mol. Simul.* **2004**, *30*, 81.
(45) (a) Vishnyakov, A.; Neimark, A. V. *J. Phys. Chem. B* **2000**, *104*, 4471. (b) Rivin, D.; Meermeier, G.; Schneider, N. S.; Vishnyakov, A.; Neimark, A. V. *J. Phys. Chem. B* **2004**, *108*, 8900.
(46) Glotzer, S. C.; Paul, W. *Annu. Rev. Mater. Res.* **2002**, *32*, 401.
(47) Mazars, M. *J. Chem. Phys.* **2001**, *115*, 2955.
(48) Paul, R.; Paddison, S. *J. Chem. Phys.* **2001**, *115*, 7753.
(49) Paddison, S.; Elliott, J. A. *J. Phys. Chem. B* **2005**, *109*, 7583.
(50) Yan, L.; Ji, X.; Lu, W. *J. Phys. Chem. B* **2008**, *112*, 5602.
(51) Chen, C. L.; Hua, C. Y.; Wu, C. R. *Macromol. Theory Simul.* **2001**, *10*, 644.
(52) Mauritz, K. A.; Moore, R. B. *Chem. Rev.* **2004**, *104*, 4535.
(53) Yang, G. *Proc. Natl. Acad. Sci. U.S.A.* **2000**, *97*, 139.
(54) Danilowicz, C. *Proc. Natl. Acad. Sci. U.S.A.* **2003**, *100*, 1694.
(55) Chourdakis, N.; Voyiatzis, G. A. *J. Polym. Sci., Part B: Polym. Phys.* **2007**, *45*, 2509.
(56) Allahyarov, E.; Taylor, P. L., submitted to *Phys. Rev. E.*
(57) Trevino, S. F.; Young, S. K. Army Research Labarotory Report, **2002**.
(58) Bagrodia, S.; Mohajer, Y.; Wilkes, G. L. *Polym. Bull.* **1982**, *8*, 281.

JP8047746